Analysis of size effects associated to the transformation strain in TRIP steels with strain gradient plasticity

L. Mazzoni-Leduc, T. Pardoen, T.J. Massart

Accepted Manuscript

Title: Analysis of size effects associated to the transformation strain in TRIP steels with strain gradient plasticity

Authors: L. Mazzoni-Leduc, T. Pardoen, T.J. Massart

PII: S0997-7538(09)00098-9

DOI: 10.1016/j.euromechsol.2009.08.001

Reference: EJMSOL 2542

To appear in: *European Journal of Mechanics / A Solids*

Received Date: 9 March 2009

Revised Date: 30 June 2009

Accepted Date: 5 August 2009

Please cite this article as: Mazzoni-Leduc, L., Pardoen, T., Massart, T.J. Analysis of size effects associated to the transformation strain in TRIP steels with strain gradient plasticity, European Journal of Mechanics / A Solids (2009), doi: 10.1016/j.euromechsol.2009.08.001

Analysis of size effects associated to the transformation strain in TRIP steels with strain gradient plasticity.

L. Mazzoni-Leduc[a], T. Pardoen[b], T.J. Massart[a]

[a] *Université Libre de Bruxelles, Building, Architecture & Town Planning Dept. (BATir) CP 194/02, Avenue F.D. Roosevelt 50, 1050 Bruxelles, Belgium*
[b] *Université catholique de Louvain, Institute of Mechanics, Materials and Civil Engineering, Place Sainte Barbe, 2, B-1348 Louvain-la-Neuve, Belgium*

Abstract

The size dependent strenghtening resulting from the transformation strain in Transformation Induced Plasticity (TRIP) steels is investigated using a two dimensional embedded cell model of a simplified microstructure composed of small cylindrical metastable austenitic inclusions within a ferritic matrix. Earlier studies have shown that within the framework of classical plasticity or of the single length parameter Fleck-Hutchinson strain gradient plasticity theory, the transformation strain has no significant impact on the overall strengthening. The strengthening is essentially coming from the composite effect with a marked inclusion size effect resulting from the appearance during deformation of new boundaries constraining the plastic flow. The three parameters version of the Fleck-Hutchinson strain gradient plasticity theory is used here in order to better capture the effect of the plastic strain gradients resulting from the transformation strain. The three parameters theory incorporates separately the rotational and extensional gradients in the formulation, which leads to a significant influence of the shear component of the transformation strain, not captured by the single parameter theory. When the size of the austenitic inclusions decreases, the overall strengthening increases due to a combined size dependent effect of the transformation strain and of the evolving composite structure. A parametric study is proposed and discussed in the light of experimental evidences giving indications on the optimization of the microstructure of TRIP-assisted multiphase steels.

Key words: Strain induced martensitic transformation, TRIP-Assisted steels, Transformation strain, Strain gradient plasticity, Computational

homogenisation.

1. Introduction

The routes for improving the strength of metallic materials towards lighter and safer structures are numerous. Aside from the many possibilities offered by alloying, pre-deforming and/or producing composite structures, microstructure refinement is one of the most versatile and powerful way to strengthen a metal. Refining microstructures means for instance reducing the grain size in order to take benefit of the well known Hall-Petch effect (Hall, 1951; Petch, 1953), limiting the precipitate size to an optimal diameter (Simar et al., 2007), decreasing the twin spacing (Dao et al., 2006), or decreasing the thickness of lamellae in lamellar structures (Huang et al., 2001; Modi et al., 2001). Another example, which is the focus of the present research, is related to microstructures involving a second phase which is metastable at operating temperature and which, under mechanical loading, transforms into a harder phase. An important class of metals involving this mechanism is known as multiphase TRIP aided steels (with TRIP standing for TRansformation Induced Plasticity) in which retained austenite inclusions transform into a hard martensitic phase during plastic deformation. A former study (Mazzoni-Leduc et al., 2008) has shown that an important contribution to the strengthening associated to the TRIP effect originates from the small size of the austenite islands typically smaller than $1 - 3\mu m$.

The size dependent strengthening associated to microstructure refinement can be related to the presence of geometrically necessary dislocations and to the associated large strain gradients needed for the compatibility of the deformation. Strain gradients effects and the principle of "smaller being stronger" is also observed in another class of problems involving homogenous solids loaded heterogeneously, such as in torsion of thin wires (Fleck et al., 1994), bending of thin strips (Stölken and Evans, 1998), micro- or nano-indentation with the hardness increasing with decreasing indentation depth (Ma and Clarke, 1995; McElhaney et al., 1998; Elmustafa and Stone , 2002; Swadener et al., 2002; Delincé et al., 2006). In these classes of problems, large plastic strain gradients develop within regions smaller than a few microns and the density of geometrically necessary dislocations leads to a significant hardening contribution as well as an associated back stress or kinematic hardening contribution. In wire torsion, thin strip bending, and

nanoindentation, strain gradients are caused by the loading configuration and the small sample size. In microstructure controlled strengthening, plastic strain gradients essentially develop due to the presence of impenetrable (or partially impenetrable) boundaries, causing, for the sake of compatibility, excess dislocations to pile up and accumulate in small regions.

Among the phenomenological strain gradient plasticity theories, the one proposed by Fleck and Hutchinson (Fleck and Hutchinson, 2001) is a higher order theory which, on top of accounting for the effect of the strain gradients, requires higher order stress quantities and boundary conditions, capable of capturing the response of impenetrable boundaries. This formulation offers a good trade off between the complexity of 3D Discrete Dislocation Dynamics in terms of computational time (see e.g. Devincre and Robert, 1996) and more simple size dependent theories but which do not incorporate higher order variables, and thus offer no option for imposing higher order boundary conditions (e.g. Acharya and Bassani, 2000). Note that another class of theories, as developed for instance by Evers et al. (2004) and Geers et al. (2007), introduce the effect of the impenetrable boundaries by adding in the formulation a back stress related to the plastic incompatibility. Kuroda and Tvergaard (2008) have recently shown that this last class of non work conjugate theories is, under some assumptions, similar mathematically to the higher order conjugate theories of the class developed by Fleck and Hutchinson in the case of a crystal plasticity formulation.

The motivations for investigating the TRansformation Induced Plasticity occuring in multi-phase steels using strain gradient plasticity theory are the following. Under mechanical loading, a fraction of the austenitic phase transforms into martensite generating internal stresses and an accumulation of geometrically necessary dislocations around the transformed region (see e.g. Jacques, 2004). As a result, an increase of the overall strengthening takes place via three mechanisms (e.g. Fischer and Reisner, 1998; Fischer et al., 2000; Furnémont, 2003; Lani et al., 2007):

- the increase of the volume fraction of the harder martensitic phase contributing to an elevation of the global hardening through a size independent composite type effect;
- the generation of extra dislocations around the transformed regions required to accomodate the relatively large transformation strain occurring in the transforming zone;

- the appearance of a new boundary at the frontier of the martensitic phase, impenetrable to dislocations, leading, during further deformation, to an extra hardening in the region surrounding the transforming zone of the material.

In a previous study (Mazzoni-Leduc et al., 2008), the authors investigated the TRIP effect based on an FE implementation of the single parameter version of the Fleck-Hutchinson theory to describe the plasticity of the different phases. A key ingredient was the formulation of evolving boundary conditions at the interface between the austenite and the newly formed martensite plate, free before transformation and impenetrable after transformation. This former study has shown that:

- The use of the strain gradient plasticity theory leads to much larger strengthening related to the TRIP effect than when using classical plasticity theory, in better qualitative agreement with experimental observations.

- Decreasing the size of the austenitic inclusion increases the strengthening. The behaviour of the martensitic phase is also affected, since the martensite undergoes compressive stresses during the transformation. The recovery after transformation during additional deformation of a tensile stress state is delayed when the size of the austenitic inclusion decreases, which is important with respect to damage nucleation.

- The boundary conditions specified at the boundary of the plastically deforming region play a major role on the impact of the transformation strain on the strength of the material. When the plastic flow is unconstrained at the elasto-plastic boundaries (except at the austenite/martensite interface), the transformation strain has only a very weak effect on the strengthening whatever the size and volume fraction of retained austenite. Most of the strengthening comes from the evolving composite effect associated to the presence of a new hard inclusion. An effect of the transformation strain is captured only when the plastic flow is constrained at every elasto-plastic boundaries, an option which can hardly be motivated physically and was therefore avoided.

This last conclusion was the main motivation for investigating the three parameters version of the Fleck-Hutchinson theory. Indeed, Fleck and Hutchinson (2001) state that the three parameters version of the theory should be

used for cases embracing both stretch and rotation gradients. For instance, Niordson and Hutchinson (2003b) show that the modelling of the shearing of a finite slab with the three parameters version of the theory leads to much larger strengthening compared to the single parameter theory. This extra-hardening originates from the fact that the full tensor of the gradients of plastic strains is incorporated in the formulation, which induces a non-zero gradient contribution at the free edges (from the natural boundary condition on plastic flow), whereas the single parameter theory only involves the gradient of effective plastic strain rate, with no contribution of the plastic gradients at the free edges. Determining whether or not, based on a more physical theory, significant strengthening can result from the transformation strain and to what extent it is also size dependent is essential with respect to further microstructure optimization efforts. Considering the complexity of the microstructure and the number of parameters, it is indeed important for metallurgists to be guided in their developments of improved TRIP steels regarding, among others, the optimum austenite grain size.

The outline of the paper is the following. Section 2 describes the modelling assumptions and summarises the three parameters formulation. A parametric study of a simplified microstructure is presented in Section 3. In order to set the stage of the analysis, the central question which will be asked is: among the three length parameters, which one(s) will have the stronger effect in the strengthening related to the phase transformation? Specific attention is given to the influence of (i) the effect of each of the length parameters entering the formulation of the Fleck-Hutchinson strain gradient plasticity theory, (ii) the transformation strain, (iii) the size of the austenitic inclusions. The results are discussed in Section 4 with an emphasis on the behaviour at the elasto-plastic boundaries.

2. Model

2.1. Mechanical modelling of the phase transformation

Since the retained austenitic phase is metastable at room temperature, it can transform under deformation into the harder martensitic phase. The following notations, classical in physical metallurgy, will be used throughout the paper

$$\alpha \rightarrow \text{ferrite}, \qquad \alpha' \rightarrow \text{martensite}, \qquad \gamma \rightarrow \text{austenite},$$
$$HOM \rightarrow \text{homogenized medium}.$$

For the sake of comparison with earlier works (see Mazzoni-Leduc et al., 2008), the same representative microstructure element, described in Figure 1a, will be modelled in two dimensions under plane strain tensile loading conditions. The cell element is composed of a cylindrical austenitic inclusion surrounded by a ferritic matrix. An elliptical transforming zone is considered into the austenite inclusion with a martensitic variant oriented at 45° with respect to the tensile axis, see Van Rompaey et al. (2006). The volume fraction of the transforming zone is in principle controlled by the phase transformation condition, which is, in turn, directly affected by details of the microstructure arrangement and by the balance of driving and resistive forces. Modelling explicitely the nucleation and growth of the martensitic phase is outside the scope of this study (see e.g. Fischer and Reisner, 1998; Reisner et al., 1998; Fischer et al., 2000). The final volume of the martensitic zone is imposed in the simulation and the transformation is assumed to occur homogenously within the lenticular plate with a realistic overall volume fraction of 3.3%, see Jacques (2004). The appearance of other plates, and associated interaction effects, is not modelled here, see Marketz and Fischer (1995). The stress-free transformation strain consists of a shear γ^{tsf} and a dilatation δ^{tsf} component along the small axis of the plate, and has the following form in the local axis (1,2) of the lenticular plate, see Fig. 1a:

$$\varepsilon_{loc}^{tsf} = \begin{bmatrix} 0 & 0 & 0 \\ 0 & 0 & \gamma^{tsf}/2 \\ 0 & \gamma^{tsf}/2 & \delta^{tsf} \end{bmatrix}. \tag{1}$$

The deformation process is modelled in three stages.

Step 1 The cell is first loaded until the overall strain E reaches the strain prescribed for the onset of transformation E_{tsf}^{start}. This value corresponds to an average strain $< \varepsilon >_{tsf,\gamma}^{start}$ in the austenite. Since the strength mismatch is not very large between austenite and ferrite, $< \varepsilon >_{tsf,\gamma}^{start}$ does not differ too much from E_{tsf}^{start}. The corresponding overall stress Σ is noted Σ_{tsf}^{start}.

Step 2 An artificial thermal loading stage is then applied with a variation of temperature ΔT associated to fictitious thermal expansion coefficients α_{ij} in order to impose the transformation strain ε_{loc}^{tsf} to the transforming region. The material properties are gradually modified following a

linear variation with ΔT.

Step 3 The mechanical loading is resumed.

The loading conditions on the cell represented in Fig. 1a have a strong impact on the response of the representative cell, at least during the transient regime following the transformation. The homogenisation of a conventional unit cell usually requires the choice of the macroscopic quantities controlling the loading. Usually, the average stress or average strain is prescribed on the unit cell. Nevertheless, during the phase transformation, the representative evolution of the average stress or strain on the unit cell (and the related tractions or displacement at its boundary) is unknown. The response of the unit cell is actually intermediate between these two extreme assumptions of constant load or constant deformation, and depends on the exact resistance of the surrounding medium. In order to avoid explicit imposition of mechanical quantities at the boundary, the unit cell is embedded into an equivalent continuum, in order to make the transformation stage independent of the mechanical control on the cell, see Van Rompaey et al. (2006) and Mazzoni-Leduc et al. (2008). The mechanical control of the model is thereby transferred to the boundary of this surrounding region. The transformation can then occur under an imposed far field constant stress or strain leading to identical results after the transformation transient by leaving the average stress on the unit cell free to adjust to the evolving microstructural behaviour. Practically, the unit cell is embedded in a surrounding composite with the same uniaxial behaviour as the one obtained by averaging the behaviour of a unit cell without transformation, and on which the overall mechanical loading is applied (E_{far} or Σ_{far}), as shown on Fig. 1b. The response of such an embedded cell model is intermediate between the two extreme behaviours of the unit cell model, under constant Σ or constant E (Mazzoni-Leduc et al., 2008). The response of the transforming unit cell is then obtained by averaging the stress and strain over the volume of the central unit cell:

$$E_{cell} = \frac{1}{V_{cell}} \int_{V_{cell}} \varepsilon \mathrm{d}V_{cell} \,, \qquad \Sigma_{cell} = \frac{1}{V_{cell}} \int_{V_{cell}} \sigma \mathrm{d}V_{cell} \,. \tag{2}$$

2.2. Strain gradient plasticity model

The three length parameter version of the Fleck-Hutchinson strain gradient plasticity theory (Fleck and Hutchinson, 2001) has already been used

to address several problems such as whisker-reinforced metals (Niordson, 2003a), plastic localization (Niordson and Tvergaard, 2005), or, in the original paper, wire torsion and void growth (Fleck and Hutchinson, 2001). The essentials are summarized here, within a small strain formulation.

2.2.1. Generalized effective plastic strain rate

As for classical plasticity theory, the higher order theory is based on the usual definition of the conventional effective plastic strain rate $\dot{\epsilon}_P$

$$\dot{\epsilon}_P = \sqrt{2\dot{\epsilon}^P_{ij}\dot{\epsilon}^P_{ij}/3}\,. \tag{3}$$

The von Mises effective stress is expressed as $\sigma_e = \sqrt{\frac{3}{2}s_{ij}s_{ij}}$, where s_{ij} is the deviatoric part of the Cauchy stress tensor. The direction of the plastic strain increment is defined as $m_{ij} = 3s_{ij}/2\sigma_e$ and the plastic strain rate tensor is expressed as $\dot{\epsilon}^P_{ij} = \dot{\epsilon}_P m_{ij}$. The plastic strain gradient tensor is defined as

$$\rho_{ijk} = \dot{\epsilon}^P_{ij,k}\,. \tag{4}$$

The incompressibility of plastic deformation together with the symmetry of the plastic deformation tensor allows splitting ρ_{ijk} into a unique sum of three orthogonal tensors $\rho^{(m)}_{ijk}$ for $m = [1, 3]$, obeying the incompressibility requirement and showing the same symmetry condition as ρ_{ijk} (Smyshlyaev and Fleck, 1996). This allows the identification of the three homogeneous invariants of degree two of the plastic strain gradient tensor as $\rho^{(m)}_{ijk}\rho^{(m)}_{ijk}$ for $m = [1, 3]$. The expression of the generalized effective plastic strain incorporating all gradient terms of the plastic strain rate via these three invariants reads:

$$\dot{E}^2_P = \dot{\epsilon}^2_P + l^2_1\rho^{(1)}_{ijk}\rho^{(1)}_{ijk} + 4l^2_2\rho^{(2)}_{ijk}\rho^{(2)}_{ijk} + 8/3l^2_3\rho^{(3)}_{ijk}\rho^{(3)}_{ijk} \tag{5}$$

where the three lengths scales l_1, l_2 and l_3 come as a result of dimensional consistency. These length parameters set the scale at which plastic strain gradients will have an impact on the response of the medium. The coefficients 4 and 8/3 are required for connection with earlier works of the authors (Fleck and Hutchinson, 1997), in which the complete strain gradient tensor is involved. A simplified version of the theory, involving only one parameter l_*, recovers the initial Aifantis theory (Aifantis, 1984), as used in Mazzoni-Leduc et al. (2008). In this case, the generalized effective plastic strain rate is calculated via a quadratic sum of the plastic strain gradient components:

$$\dot{E}^2_P = \dot{\epsilon}^2_P + l^2_*\dot{\epsilon}_{P,i}\dot{\epsilon}_{P,i}\,. \tag{6}$$

Rewriting the plastic strain gradient tensor as a function of the effective plastic strain rate, the direction of plastic flow and their gradients as follows

$$\rho_{ijk} = \dot{\epsilon}_{P,k} m_{ij} + \dot{\epsilon}_P m_{ij,k} \tag{7}$$

allows recasting Equation (5) into a form depending on the effective plastic strain rate, its gradients and the coefficients A_{ij}, B_i and C

$$\dot{E}_P^2 = \dot{\epsilon}_P^2 + A_{ij}\dot{\epsilon}_{P,i}\dot{\epsilon}_{P,j} + B_i\dot{\epsilon}_{P,i}\dot{\epsilon}_P + C\dot{\epsilon}_P^2 \tag{8}$$

where the expressions of the coefficients A_{ij}, B_i and C can be evaluated from the direction of plastic flow m_{ij} and its gradients, and from the three internal lengths. The explicit form of the coefficients is given by (Fleck and Hutchinson, 2001)

$$\begin{aligned}
A_{ij} = \;& l_1^2(\delta_{ij}/2 + 2/5 m_{ip}m_{jp}) + L_2^2(3/2\delta_{ij} - m_{qi}m_{qj}) + L_3^2(e_{pir}e_{qjv}m_{qr}m_{pv}) \\
B_i = \;& 4/3 l_1^2 m_{pq}m_{pi,q} - 8/15 l_1^2 m_{ip}m_{pq,q} - 2L_2^2 m_{qr}m_{qi,r} + 2L_3^2 e_{quv}e_{pir}m_{qr}m_{pv,u} \\
C = \;& l_1^2/3(m_{ij,k}(m_{ij,k} + 2m_{jk,i}) - 4/5 m_{ki,i}m_{kj,j}) + L_2^2(m_{qr,u}m_{qr,u} - m_{qr,v}m_{qv,r}) \\
& + L_3^2 e_{pir}e_{quv}m_{qr,i}m_{pv,u}
\end{aligned} \tag{9}$$

with $L_2^2 = 4/3 l_2^2 + 8/5 l_3^2$ and $L_3^2 = 4/3 l_2^2 - 8/5 l_3^2$.

In contrast with the one parameter theory, relations (8) and (9) show that the stress state and its gradients appear in the gradient enhancement through the plastic flow direction and its gradients, leading to distinct effects of the rotational and stretch gradients. Within the Fleck and Hutchinson approach, l_1 is active for both stretch and rotation gradients, while l_2 and l_3 are related only to rotation gradients (Fleck and Hutchinson, 2001).

The generalized effective plastic strain rate is intended to be a phenomenological measure of the total density of dislocations, composed of the statistically stored dislocations (SSD) and geometrically necessary dislocations (GND). The statistically stored dislocations (SSD) accomodate homogenous plastic strain fields, and accumulate by trapping each other randomly. The SSD density is commonly assumed to be represented by the effective plastic strain ε_P (Fleck et al., 1994; Nix and Gao, 1997; Huang et al., 2004; Brinckmann et al., 2006) while the geometrically necessary dislocations (GND), required to accomodate inhomogenous plastic deformation and to guarantee lattice compatibility are related to the plastic strain gradients (Fleck et al., 1994; Arsenlis and Parks, 1999; Mughrabi, 2004; Abu Al-Rub and Voyiadjis, 2006).

2.2.2. Governing and constitutive equations

The incremental principle of virtual work reads for each incremental displacement $\delta\dot{u}_i$ and effective plastic strain rate $\delta\dot{\epsilon}_P$ (Fleck and Hutchinson, 2001):

$$\begin{array}{l} \forall\delta\dot{u}_i, \forall\delta\dot{\epsilon}_P \\ \int_V \left\{ \dot{\sigma}_{ij}(\delta\dot{\varepsilon}^e_{ij} + \delta\dot{\varepsilon}^*_{ij}) + \dot{Q}\delta\dot{\varepsilon}_P + \dot{\tau}_i\delta\dot{\varepsilon}_{P,i} \right\} dV = \int_S \left(\dot{T}_i\delta\dot{u}_i + \dot{t}\delta\dot{\varepsilon}_P \right) dS \end{array} \tag{10}$$

in which a transformation strain ε^*_{ij}, being non zero only in the transforming zone has been introduced; Q is the generalized effective stress, work-conjugate to the plastic strain rate $\dot{\varepsilon}_P$ and τ_i is a higher order stress work-conjugate to the gradient of the effective plastic strain rate $\dot{\varepsilon}_{P,i}$. In the absence of body forces, straightforward manipulations lead to the strong form of the field equations

$$\dot{\sigma}_{ij,j} = 0 \tag{11}$$

which is the equilibrium equation, and

$$\dot{\sigma}_e = \dot{Q} - \dot{\tau}_{i,i} \, . \tag{12}$$

Equation (12) is a generalized consistency equation only valid in the plastic regime. The boundary conditions associated to this system of equations are

$$\begin{array}{c} \dot{T}_i = \dot{\sigma}_{ij} n_j \, , \\ \dot{t} = \dot{\tau}_i n_i \, . \end{array} \tag{13}$$

To close the formulation, the incremental constitutive equations are given by

$$\begin{array}{l} \dot{\sigma}_{ij} = L_{ijkl}(\dot{\epsilon}_{kl} - \dot{\epsilon}^P m_{kl} - \dot{\varepsilon}^*_{kl}), \\ \dot{\tau}_i = h(E_P)(A_{ij}\dot{\epsilon}_{P,j} + 1/2 B_i \dot{\epsilon}_P), \\ \dot{Q} = h(E_P)(\dot{\epsilon}_P + 1/2 B_i \dot{\epsilon}_{P,i} + C\dot{\epsilon}_P), \end{array} \tag{14}$$

where L_{ijkl} denotes the elastic stiffness tensor for an isotropic solid and h is the hardening rate which is defined by

$$h = \left. \frac{\mathrm{d}\sigma_{\mathrm{y}}(\kappa)}{\mathrm{d}\kappa} \right|_{E_P} \tag{15}$$

where $\sigma_y(\kappa)$ is the hardening law and κ is the hardening parameter measuring the accumulation of dislocations. The hardening is evaluated at $\kappa = E_P$ rather than at $\kappa = \varepsilon_P$ to take into account the contribution of the GNDs

associated to the plastic gradients. The consistency equation governing plastic flow is then expressed through the generalized effective stress by $Q = Q_y$ where the evolution of Q_y is given by:

$$\dot{Q}_y = h(E_P)(\dot{\epsilon}_P + 1/2 B_i \dot{\epsilon}_{P,i} + C\dot{\epsilon}_P) \; . \tag{16}$$

2.2.3. Implementation issues

In this study, a purely incremental (or explicit) implementation of the formulation similar to the one presented in Niordson and Hutchinson (2003b) is used. Small time steps are therefore needed to limit departure from the exact solution. The convergence with respect to time step and mesh refinement has therefore been systematically verified.

The Fleck and Hutchinson (2001) three parameters theory has been implemented in a finite element code using C^0 quadrangular and triangular elements. The displacement rate field and the effective plastic strain rate field are interpolated using bi-quadratic and bi-linear functions, respectively. The elastic-plastic transition is tested at each Gauss point. When the von Mises stress at a Gauss point which was elastic during the previous time step becomes larger than the yield stress, the Gauss point is considered to enter the plastic regime. Elastic unloading occurs whenever the effective plastic strain rate calculated at a plastic Gauss point is negative (see Niordson and Hutchinson, 2003b).

Due to the dependence of the coefficients A_{ij}, B_i and C on the gradients of the direction of plastic flow $m_{ij,k}$, the computation of the gradient enhancement of the generalized effective plastic strain requires a specific treatment. The calculation of $m_{ij,k}$ for the next step necessitates a smoothing of the stress field to compute the derivatives $s_{ij,k}$. The gradients of the direction of plastic flow, $m_{ij,k}$, are then evaluated according to the relation

$$m_{ij,k} = \frac{1}{2} \frac{s_{ij,k}\sigma_e - s_{ij}\frac{3}{2}\frac{s_{pq}s_{pq,k}}{\sigma_e}}{\sigma_e^2} \; . \tag{17}$$

The procedure for the construction of a continuous stress field entering the expression of the three coefficients described in Niordson and Hutchinson (2003b) is adopted. For each element, after having determined the increments of the displacements and of the effective plastic strain, the constitutive equations are integrated at each Gauss point. The stresses are subsequently extrapolated at each corner node. For each corner node, an average value

of the stress is determined from the contribution of the elements connected to the node. The averaged nodal values of the stress field are then interpolated using bilinear shape functions at the centre of the element, where the stress derivatives and subsequently the coefficients A_{ij}, B_i and C are evaluated and attributed to all the Gauss points of the element. Note that the same smoothing procedure was used in other works with various interpolation schemes [3-5]. In order to verify that the results do not depend on the smoothing procedure, other procedures were tested, attributing different gradient coefficients to the different Gauss points of an element. No difference was found in the results provided the mesh is fine enough.

2.3. Evolving plastic boundary conditions

Since the formulation uses an independent effective plastic strain rate field, higher order boundary conditions must be specified at the external boundary of a region where plastic flow occurs. Two extreme types of conditions can be considered (see Niordson and Hutchinson, 2003b):

- at a free surface, dislocations move through unimpeded. No constraint on the effective plastic strain rate $\dot{\epsilon_P}$ should then be applied, which is equivalent to the natural boundary condition on the higher order traction, i.e. $\dot{\tau}_i n_i = 0$.

- at a strongly bonded interface, or an interface between phases, dislocations accumulate in the near interface region. The boundary condition corresponding to a boundary impenetrable to dislocations is $\dot{\varepsilon}_P = 0$.

The evolving nature of the interface between austenite and the newly formed martensite domain requires changing the boundary conditions in the course of the simulation. The plastic flow is therefore suddenly constrained along the interface by setting the rate of effective plastic strain equal to zero i.e. $\dot{\epsilon_P} = 0$ at the onset of the transformation.

Finally, boundary conditions must be prescribed also along the elastic-plastic boundary. Again, the two choices of boundary conditions described above are possible. The choice is not so obvious (see e.g. Peerlings, 2007) although the physics calls more for the natural boundary condition $\dot{\tau}_i n_i = 0$.

A natural boundary condition will therefore be used at the moving elasto-plastic boundaries for all the computations reported in this paper. This choice is motivated by the fact it provides a lower bound of the size effects associated to the transformation. Note that the same assumption is used at

the boundary between the unit cell and the surrounding composite which is represented by a classical continuum description.

3. Results

A study of the main parameters of the problem is performed with the embedded cell model described in subsection 2.1. A mesh containing 11744 elements has been used for the generation of all the results presented in this paper. while imposing plane strain conditions and the interpolations defined in Section 2.2.3. Quadrangular elements were used within the ferritic phase, and triangular elements in the inclusion. The convergence of the results with respect to the mesh size was verified using even finer meshes. First, the choice of the material and loading parameters are described. The parametric study starts by showing the individual effects of the different gradient terms on the overall transformation hardening. The effect of the different gradient terms on the individual transformation hardening contributions are then separately presented with a focus on the influence of the transformation strain. The section ends with results relative to the influence of the austenitic grain size.

3.1. Material and loading parameters

All the phases are assumed to follow a Swift-type hardening law

$$\sigma_y = \sigma_{y0}(1 + \varepsilon_0 \kappa)^n \tag{18}$$

where σ_y is the current yield stress, σ_{y0} is the initial yield stress, ε_0 is the hardening coefficient, n is the strain hardening exponent, and κ is the hardening parameter. The flow parameters used for each phases are motivated from experimental and modelling efforts on a specific grade of TRIP assisted multiphase steels (Furnémont, 2003; Jacques et al., 2006, 2007), see Table 1. The behaviour of the surrounding composite is described by the classical J_2 flow theory. Some parameters are kept fixed in this study:

- the longitudinal (dilatational) transformation strain along the small axis of the lenticular plate δ^{tsf} is set equal to 3%;
- the volume fraction of the transforming zone with respect to the initial austenitic inclusion given by $\dfrac{h}{d} = \dfrac{1}{3}$, where h is the width of the lenticular plate and d is the diameter of the inclusion, see Fig. 1a;

- the volume fraction of retained austenite f_γ is equal to 10%, resulting in a global volume fraction of the transforming zone equal to 3.3%;
- the macroscopic strain level E_{tsf}^{start} at which transformation starts is equal to 2.25%.

Specific attention is given to the strength enhancements associated to the phase transformation captured when using a three parameters theory, compared to the results obtained with the single parameter theory described in details in Mazzoni-Leduc et al. (2008). The size effects will be analysed for various ratios l_i/d. Four cases are considered:

- Case n°1. No phase transformation occurs, corresponding to the response of a composite ferritic matrix/austenitic inclusion.
- Case n°2. A change of elasto-plastic properties is imposed in the transforming region accompanied by evolutive boundary conditions: the plastic flow is initially unconstrained and becomes constrained at the $\alpha^{'}/\gamma$ interface at the start of the transformation. The emergence of the new impenetrable phase boundary leads to a strengthening contribution called "higher order composite effect" in the sequel.
- Case n°3. The transformation strain is applied during the transformation on top of the changes applied in Case n°2.
- Case n°4. The transformation strain only is applied without any modification of the elastic-plastic properties of the transforming region and without any evolving boundary conditions on plastic flow at the interface of the transformed region.

The contribution of the transformation to the strengthening is described through a non-dimensional index $S(E)$ corresponding to a macrostrain E:

$$S(E) = \frac{\Sigma}{\Sigma_{ref}} \tag{19}$$

where Σ_{ref} is the average stress corresponding to the average strain E in the embedded cell within case n°1, and Σ corresponds to the average strain E in the other cases n°2, n°3 or n°4.

3.2. Separate effects of the gradient terms on the overall transformation hardening

Figure 2 illustrates the average response along the tensile direction of the embedded unit cell where the effects of the length parameters are addressed separately, i.e. with l_i/d (i varying from 1 to 3) all equal to 0 except for one normalized length equal to 1. The goal is to quantify the relative impact of the rotational and the stretch gradient terms on the global response using the most realistic description of the transformation, i.e. for case n°3. The incorporation in the formulation of the contribution of each of the invariants of the plastic strain gradient tensor $\rho^m_{ijk}\rho^m_{ijk}$ separately (m varying from 1 to 3) clearly induces more strengthening than when using the single parameter theory (with $l_*/d = 1$):

- When $l_1/d = 1$ is the only active length parameter, the strengthening at $E = 10\%$ is 1.8 times larger than when using the single parameter theory. The length l_1 is associated to stretch and rotation gradients.

- When $l_2/d = 1$ or $l_3/d = 1$ the strengthening amounts to 2.7 times the strengthening obtained with the single parameter theory at $E = 10\%$. This agrees with the results presented in (Niordson and Hutchinson, 2003b) in the case of the shearing of a finite slab with constrained plastic flow at the boundaries. Furthermore, the response is the same in the cases $l_2/d = 1$ or $l_3/d = 1$.

3.3. Effect of the gradient terms on each transformation hardening contributions

No effect of the transformation strain on the overall strengthening enhancement was observed with the single parameter theory in the case of unconstrained elasto-plastic boundaries which is the most realistic description of the problem (Mazzoni-Leduc et al., 2008). The aim of this section is to investigate whether the use of the multi-parameter theory is demonstrating any additional hardening effect resulting from the transformation strain.

In order to distinguish the effects of the transformation strain and of the change of plastic properties associated to the phase change, the responses corresponding to cases n°1, n°2 and n°3 are plotted first for different choices of internal length. Fig. 3a shows results for $l_1/d = 1$ and $l_2/d = l_3/d = 0$. The transformation strain contributes to 25% of the total strengthening (this percentage is calculated based on the ratio of the difference of stress levels

between cases n°3 and n°2 over the difference of stress levels between cases n°3 and n°1). Fig. 3b shows the results for $l_2/d = 1$ and $l_1/d = l_3/d = 0$. The extra strengthening associated to the transformation strain amounts to 36% of the total strengthening when $E = 10\%$. Note that the same trend is found for $l_3/d = 1$ and $l_1/d = l_2/d = 0$ (with a 31% increase). Again, the rotation gradients lead to larger strengthening compared to the stretch gradients.

Hence, the use of the multi-parameter framework, even when including only one of the three invariants of the plastic strain gradient rate tensor in the generalized effective plastic strain measure, leads to a significant contribution of the transformation strain. This contrasts with the results obtained with the single parameter theory.

Figure 3c gives the response obtained in cases n°1, n°2 and n°3 when all intrinsic length parameters are activated: $l_1/d = l_2/d = l_3/d = 1$. The extra hardening resulting from the higher order composite effect, caused by the evolving boundary conditions and represented by case n°2, leads to larger strengthening compared to the choice in which only one ratio l_i/d is non-zero. The transformation strain contribution represents 40% of the overall effect of the transformation on the strengthening.

Fig. 4 depicts the response obtained in cases n°1, n°2 and n°3 when γ_{tsf} varies from 0% to 20% and with all length parameters activated, i.e. $l_1/d = l_2/d = l_3/d = l/d = 1$. The influence of γ_{tsf} is obvious, especially for values of γ_{tsf} larger that 10%. The role of the dilatation component δ_{tsf}, which is equal to 3%, requires also some comments. When $E = 10\%$, it is responsible for 10% of the global increase in the hardening related to the martensitic transformation on top of the hardening enhancement due to the higher order composite effect (obtained by the ratio of the difference of stress levels between cases n°3 and n°2, on one hand and n°3 and n°1 on the other hand). When the shear component increases, rotational gradients develop, which activates the effect of the intrinsic length l_2 and l_3 and leads to larger hardening enhancements, as shown in Fig. 3a and 3b. Note that in Mazzoni-Leduc et al. (2008), no influence of the shear component of the transformation strain γ_{tsf} was found when using the single parameter theory, the transformation strain having always a negligible role when the elasto-plastic boundaries are unconstrained.

3.4. Effect of the austenitic grain size

In this subsection, the effect of the size of the austenitic grain is addressed by varying the ratio $l_i/d = l_1/d = l_2/d = l_3/d$ between 0 and 1.5. The evolution of the hardening indicator S as a function of l/d is given in Fig. 5a and 5c when E is equal 4% and 8% respectively. Three observations can be made when comparing these predictions to the results obtained within the single parameter framework (Mazzoni-Leduc et al., 2008) reported in Fig. 5b and 5d. Within the multi-parameter framework, the S-curves corresponding to cases n°3 and n°4 almost superimpose, which is not the case when using the single parameter theory. This means that within the multi-parameter theory, the change of confinement along the transforming zone as well as the change of material properties, do not add to the strengthening when compared to the strengthening obtained in case n°4 for which only the transformation strain is introduced. The contributions of the higher order composite effect and of the transformation strain effect are not additive. The duration of the transient associated to the transformation and related to the stress drop in the stress strain curves is shorter when using the three parameters theory (see Fig. 2). This directly affects the S index at $E = 4\%$ and $l/d > 0.7$: the S-value related to cases n°3 and n°4 exceeds the value related to case n°2. With the one parameter theory (Mazzoni-Leduc et al., 2008), the picture is different: the strengthening corresponding to case n°2 always exceeds cases n°3 and n°4 at $E = 4\%$, i.e. shortly after the transformation. Finally, the impact of the transformation strain when compared to the effect of the change of material properties accompanied with the evolving boundary conditions at the α'/γ interface, increases when the ratio l/d increases, while the reverse tendency is observed when using the single parameter theory. Note also that the difference between case n°3 (or case n°4) versus case n°2 increases strongly after the transient when the three parameters theory is used as shown in Fig. 5a and 5c, whereas when the one parameter theory is used, the evolution is not that significant.

Fig. 6a and 6b show, for case n°3 and for different intrinsic lengths $l/d = l_1/d = l_2/d = l_3/d$, the evolution of, respectively, the phase averaged stress $< \sigma_{\alpha'} >$ along the tensile loading direction as a function of (a) the phase averaged strain $< \epsilon_{\alpha'} >$ and of (b) the macroscopic strain E along the tensile loading direction in the martensitic phase. The level of compression attained in the lenticular plate during transformation depends on the theory: the single parameter was found to lead to a minimum level of $< \sigma_{\alpha'} >= -3400MPa$ when the ratio $l_*/d = 2$ (cf. Mazzoni-Leduc et al.

(2008)), whereas the minimum level found with the multi-parameter theory is $< \sigma_{\alpha'} >= -4600MPa$ when $l/d = 2$. The conclusion is that increasing the ratio l/d, i.e. decreasing the austenitic grain size, amplifies the compression state associated to the transformation, as observed in Fig. 6b. The transient regime also lasts longer when l/d increases, i.e. it takes longer for the martensite to restart undergoing tensile stresses after transformation. The duration of the transient is also a function of the theory: it appears that the martensite recovers a tensile state at $E = 9\%$ using the single parameter theory and $l_*/d = 0.5$ (Mazzoni-Leduc et al., 2008), while Fig. 6b shows that using the multi-parameter theory and $l_1/d = l_2/d = l_3/d = 0.5$, the martensite still undergoes a compressive state $< \sigma_{\alpha'} >= -900MPa$ at $E = 9\%$.

4. Discussion

A significant contribution of the transformation strain to the overall strengthening of the material is predicted with the multi-parameter version of the Fleck and Hutchinson (2001) theory. This strengthening was absent of the predictions obtained with the single parameter theory and, a fortiori, from cell calculations performed with a classical plasticity theory (Furnémont, 2003) or with the single length strain gradient plasticity theory (Mazzoni-Leduc et al., 2008). Fig. 5c shows that the influence of the transformation strain alone on the overall strengthening, represented by case n°4, is larger than the influence of the change of properties alone combined with the evolving nature of the α'/γ interface (case n°2) when the size of the austenitic grain decreases. Furthermore, the combination of both effects does not lead to an additive convolution. It is important to note that the experimentally measured TRIP strengthening effects can hardly be modelled with classical theories without adjusting some fitting parameters to artificially raise the strength (see e.g. Delannay et al., 2008). The results shown here provide a potential explanation for this limitation: the behaviour of real TRIP steels involving retained austenite in the micrometer diameter range is significantly affected by strain gradients effects. This size dependence additional hardening contributes thus significantly to the remarkable improvement of the strength/ductility balance. An effort is currently made to run large scale simulations with many austenite inclusions in order to allow direct comparisons with experiments (Mazzoni-Leduc et al., 2009).

Fig. 7 shows the distribution of the elastic unloading zones at the end of the transformation step using $f_\gamma = 10\%$, $h/d = \frac{1}{3}$, l/d=1, $\gamma^{tsf} = 20\%$, and

$E_{tsf}^{start} = 2.25\%$ for case n°3. These zones are located in two regions along the horizontal symmetry axis, which is also the tensile direction. In the surrounding composite, described by classical plasticity, two other unloading zones appear, located along the vertical symmetry axis of the unit cell up to the boundary of the unit cell. With the single parameter theory and $l_*/d = 1$, the end of the transformation step shows unloading zones spreading largerly into the ferrite: along both the horizontal and the vertical symmetry axes. As a result, the stress drop during transformation is smaller with the multi-parameter framework. The presence of elastically unloading zones spreading inside the softer ferritic matrix and accomodating the transformation strain is strongly related to the strengthening enhancement obtained with the strain gradient plasticity theory. Note that the shearing and compression zones are indicated in Figure 7.

Fig. 8 shows contour plots of the variation of the generalized effective plastic strain ΔE_P from the onset of the transformation till the end, using $f_\gamma = 10\%$, $h/d = \frac{1}{3}$, l/d=1, $\gamma^{tsf} = 20\%$ and $E_{tsf}^{start} = 2.25\%$ for case n°3. Compared to the results obtained with the single parameter theory characterized by $l_*/d = 1$ under the same assumptions (Mazzoni-Leduc et al., 2008), three observations must be made. First, the repartition of ΔE_P in the "shear band" is similar whether the single or the multi-parameter theory is used. Second, larger values of ΔE_P develop into the compression band within the multi-parameter framework. The dilatation component of the transformation strain generates higher values of the effective plastic strain when the multi-parameter framework is used. Third, as a consequence of the natural boundary condition on the higher order traction $\dot{t} = (A_{ij}\dot{\epsilon}_{P,i} + B_i\epsilon_P)n_i = 0$, an implicit confinement effect on ϵ_P appears at the unconstrained elasto-plastic boundary with the multi-parameter framework. As a consequence, larger values of ΔE_P are found at the elasto-plastic boundaries as shown on Fig. 8. Contrarily, when using the single parameter theory, no confinement effect occur at the unconstrained elastic-plastic boundary. Indeed, the natural boundary condition at a traction-free boundary reads $\dot{t} = \dot{\epsilon}_{P,i}n_i = 0$. Thus, the gradient of the effective plastic strain along the normal to the elasto-plastic boundary vanishes, while the gradient along the direction tangent to the boundary is always vanishing by continuity of the effective strain rate field. Therefore, no gradient effect contributes to increase the value of ΔE_P at the unconstrained elasto-plastic boundaries when the single-parameter theory is employed. In the multi-parameter framework, all the terms of the

plastic strain rate gradient $\dot{\epsilon}^P_{ij,k}$ enter the formulation and contribute during the transformation to the confinement. This manifests into additional plastic straining related to the transformation, contributing to the increase of ΔE_P in the compression area, subjected to higher confinement between the elastic unloading zones. As a result, the multi-parameter theory leads to a higher strengthening enhancement related to the transformation strain effect, not captured when using a single parameter theory. Note that such an implicit confinement ($\dot{t} = 0$) also occurs at the boundary between the unit cell, described by the strain gradient theory, and the surrounding composite, described by classical plasticity and thus in which the higher order traction is equal to zero. It can however be seen from Figure 8 that this implicit confinement effect at the cell boundary is much lower than at the boundary of the elastically unloading zone, and does not contribute significantly to the effect related to the transformation.

The analysis of the shearing of a finite slab presented in Niordson and Hutchinson (2003b) helps understanding the behaviour of the shearing zone along the diagonal of the embedded unit cell: a slab of height $2H$ and length $2L$, such that $L/H = 1$, is considered under plane strain conditions. The top and bottom edges are bonded to rigid platens that are displaced horizontally, and behave as constrained boundaries for the plastic flow. The right and left edges are traction free. The most active lengths are l_2 and l_3 which separately lead to the same responses, exactly as obtained in the present study. Moreover, in Niordson and Hutchinson (2003b), the authors note that the strengthening increase related to the use of the three parameters theory comes from the measures of the strain gradients entering the formulation, which manifest especially at the traction-free ends where a natural boundary condition on the higher order traction incorporates an implicit confinement of the plastic flow contrarily to the single parameter theory. This observation can also be made in the present study as shown above, based on Fig. 8, where the boundary of the unloading zone acts similarly as the free edges of the finite slab, while the martensitic boundary acts as an explicitely constrained edge for the plastic unknowns.

5. Conclusions

The strengthening associated to the transformation induced plasticity (TRIP) effect within a simplified globular microstructure has been addressed using the multi-parameter Fleck and Hutchinson (2001) strain gradient plas-

ticity theory. A cell made of a ferrite matrix and an austenite inclusion is embedded into an homogenized medium. A portion of the austenite is forced to transformation into a hard martensitic plate with a change of mechanical properties as well as a transformation strain. The transformation gives rise to a hard interface at the α'/γ boundary affecting the load transfer and the plastic deformation in the vicinity. The important outcomes of this study are the following:

- The multi-parameter version of the strain gradient plasticity theory leads to much larger strengthening related to the TRIP effect compared to the single-parameter version. Note that the strengthening predicted with a classical plasticity theory is quite weak and unable to explain the experimentally observed improvements of properties.

- The use of the multi-parameter version of the strain gradient plasticity theory leads to a significant contribution to the overall strengthening of the transformation strain. The resulting hardening enhancement is mainly due to the shear component γ^{tsf} which induces rotational gradients. Therefore, the most active lengths are l_2 and l_3. No transformation strain effect is predicted with the single parameter theory except for (unrealistic) constrained elasto-plastic boundaries.

- The use of the multi-parameter version of the strain gradient plasticity theory implicitely induces a confinement at the elasto-plastic boundaries as a result of natural boundary conditions on the effective plastic strain field, which is also partly responsible for the transformation strain effect.

Further works will focus on extensions to a finite strains setting. In the study presented above, obtained with a small strain framework, the macroscopic stress level attains $1800MPa$ at the end of the computation, i.e. when $E = 10\%$, when $l/d = l_1/d = l_2/d = l_3/d = 1$ and for case n°3, which meets the commonly expected mechanical characteristic for such grades of steels. The results obtained when using a finite strain framework will give an idea of the level of ductility at higher strains. In this context, the objective for the steel industry is to reach $1800MPa$ for a macroscopic strain equal to 30% before fracture. As the transformation strain effect increases strongly when γ^{tsf} is larger than 10%, the use of finite strain framework would definitely be needed to obtain meaningful results with respect to experimental comparisons.

Acknowledgements

Financial support from Region Wallonne through the convention RW-WINNOMAT program under grant ACIETRIP 0415961 is gratefully acknowledged.

References

Abu Al-Rub, R. K., Voyiadjis, G. Z., 2006. A physically based gradient plasticity theory. International Journal of Plasticity 22 (4), April 2006, Pages 654-684

Acharya, A., Bassani, J.L., 2000. Lattice incompatibility and a gradient theory of crystal plasticity. Journal of the Mechanics and Physics of Solids 48, 15651595.

Aifantis, E.C., 1984. On the microstructural origin of certain inelastic models. Transactions of the ASME. Journal of Engineering Materials and Technology 106 (4), 326-330.

Arsenlis, A., Parks, D. M., 1999. Crystallographic aspects of geometrically-necessary and statistically-stored dislocation density. Acta Materialia 47 (5), 1597-1611.

Brinckmann, S., Siegmund, T., Huang, Y., 2006. A dislocation density based strain gradient model. International Journal of Plasticity 22 (9), 1784-1797.

Chen, S.H., Liu, L., Wang, T.C., 2007. Small scale, grain size and substrate effects in nano-indentation experiment of filmsubstrate systems. International Journal of Solids and Structures 44 (13), 4492-4504.

Dao, M., Lu, L., Shen, Y.F., Suresh, S., 2006. Strength, strain-rate sensitivity and ductility of copper with nanoscale twins. Acta Materialia 54 (20), 5421-5432.

Delannay, L., Jacques, P., Pardoen, T., 2008. Modelling of the plastic flow of trip-aided multiphase steel based on an incremental mean-field approach. International Journal of Solids and Structures 45 (6), 1825-1843.

Delincé, M., Jacques, P.J., Pardoen, T., 2006. Separation of size-dependent strengthening contributions in fine-grained Dual Phase steels by nanoindentation. Acta Materialia 54 (12), 3395-3404.

Devincre, B., Roberts, S.G., 1996. Three-Dimensional simulation of dislocation-crack interactions in bcc metals at the mesoscopic scale. Acta Materialia 44 (7), 2891-2900.

Elmustafa, A. A., Stone, D. S., 2002. Indentation size effect in polycrystalline F.C.C. metals. Acta Materialia 50 (14), 3641-3650.

Evers, L.P., Brekelmans, W.A.M., Geers, M.G.D., 2004. Non-local crystal plasticity model with intrinsic SSD and GND effects. Journal of the Mechanics and Physics of Solids 52 (10), 2379-2401.

Fischer, F. D., Reisner, G., 1998. A criterion for the martensitic transformation of a microregion in an elasticplastic material. Acta Materialia 46 (6), 2095-2102.

Fischer, F. D., Reisner, G., Werner, E., Tanaka, K., Cailletaud, G., Antretter, T., 2000. A new view on transformation induced plasticity (TRIP). International Journal of Plasticity, 16 (7-8), 723-748.

Fleck, N.A., Muller, G.M., Ashby, M.F., Hutchinson, J.W., 1994. Strain gradient plasticity: Theory and experiment. Acta Metallurgica et Materialia 42 (2), 475-487.

Fleck, N.A., Hutchinson, J.W., 1997. Strain gradient plasticity. Advances in Applied Mechanics 33, 295-361.

Fleck N.A., Hutchinson J.W., 2001. A reformulation of strain gradient plasticity. Journal of the Mechanics and Physics of Solids 49, 2245-2271.

Furnémont, Q., 2003. The micromechanics of TRIP-assisted multiphase steels. PhD thesis, Université catholique de Louvain, Louvain-la-Neuve.

Geers, M.G.D., Brekelmans, W.A.M., Bayley, C.J., 2007. Second-order crystal plasticity: internal stress effects and cyclic loading. Modelling and Simulation in Materials Science and Engineering 15, 133-145.

Huang, Y, Qu, S., Hwang, K. C., Li, M, Gao, H., 2004. A conventional theory of mechanism-based strain gradient plasticity. International Journal of Plasticity 20 (4-5), 753-782.

Jacques, P. J., 2004. Transformation-induced plasticity for high strength formable steels. Current opinion in solid state and material science 8 (3-4), 259-265.

Jacques, P. J., Furnemont, Q., Godet, S., Pardoen, T., Conlon, K. T., Delannay, F., 2006. Micromechanical characterisation of TRIP-assisted multiphase steels by in situ neutron diffraction. Philosophical Magazine 86 (16), 2371-2392.

Jacques, P.J., Furnémont, Q., Lani, F., Pardoen, T., Delannay, F., 2007. Multiscale mechanics of TRIP-assisted multiphase steels: I. Characterization and mechanical testing. Acta Materialia 55 (11), 3681-3693.

Kuroda, M., Tvergaard, V., 2008. On the formulations of higher-order strain gradient crystal plasticity models. Journal of the Mechanics and Physics of Solids, 56 (4), 1591-1608.

Hall, E.O., 1951. The Deformation and Ageing of Mild Steel: III Discussion of Results. Proceedings of the Physical Society B 64, 747-753.

Huang, B.Y., He, H.Y., Wang, J.N., 1999. Improvement in mechanical and oxidation properties of TiAl alloys with Sb additions. Intermetallics 7 (8), 881-888.

Lani, F., Furnémont, Q., Van Rompaey, T., Delannay, F., Jacques, P.J., Pardoen, T., 2007. Multiscale mechanics of TRIP-assisted multiphase steels: II. Micromechanical modelling. Acta Materialia 55 (11), 3695-3705.

Ma, Q., Clarke, D.R., 1995. Size dependent hardness of silver single crystals. Journal of Materials Research 10 (4), 853-863.

McElhaney, K.W., Vlassak, J.J., Nix, W.D., 1998. Determination of indenter tip geometry and indentation contact area for depth-sensing indentation experi-

ments. Journal of Materials Research 13 (5), 13001306.
Marketz, F., Fischer, F.D., 1995. A mesoscale study on the thermodynamic effect of stress on martensitic transformation. Metallurgical and Materials Transactions A 26 (2), 267-278.
Mazzoni-Leduc, L., Pardoen, T., Massart, T.J., 2008. Strain gradient plasticity analysis of transformation induced plasticity in multiphase steels. International Journal of Solids and Structures 45 (20), 5397-5418.
Mazzoni-Leduc, L., Pardoen, T., Massart, T.J, Strain gradient plasticity analysis of temperature dependent ductility in multiphase steels, in preparation.
Modi, O.P., Deshmukh, N., Mondal, D.P., Jha, A.K., Yegneswaran, A.H., Khaira, H.K., 2001. Effect of interlamellar spacing on the mechanical properties of $0.65\%C$ steel. Materials Characterization 46 (5), 347-352.
Mughrabi, 2004. On the current understanding of strain gradient plasticity. Materials Science and Engineering A 387-389, 209-213.
Niordson, C.F., 2003a. Strain gradient plasticity effects in whisker-reinforced metals. Journal of the Mechanics and Physics of Solids 51 (10), 1863-1883.
Niordson, C.F., Hutchinson, J.W., 2003b. Non-uniform plastic deformation of micron scale objects. International Journal for Numerical Methods in Engineering 56, 961-975.
Niordson, C.F., Redanz, P., 2004. Size effects in plane strain sheet necking. Journal of the Mechanics and Physics of Solids 52 (11), 2431-2454.
Niordson, C.F., Tvergaard, V., 2005. Instabilities in power law gradient hardening materials. International Journal of Solids and Structures, 42, 2559-2573.
Nix, D.N., Gao, H., 1997. Indentation size effects in crystalline materials: a law for strain gradient plasticity. Journal of the Mechanics and Physics of Solids 46 (3), 411-425.
Peerlings, R.J.H., 2007. On the role of moving elasticplastic boundaries in strain gradient plasticity. Modelling and Simulation in Materials Science and Engineering 15, S109-S120.
Petch, N.J., 1953. The cleavage strength of polycrystals. J. Iron and Steel Institute 174, 25-28.
Reisner, G., Werner, E. A., Fischer, F. D., 1998. Micromechanical modeling of martensitic transformation in random microstructures. International Journal of Solids and Structures 35 (17), 2457-2473.
Simar, A., Bréchet, Y., de Meester, B., Denquin, A., Pardoen, T., 2007. Sequential modeling of local precipitation, strength and strain hardening in friction stir welds of an aluminum alloy 6005A-T6. Acta Materialia 55 (18), 6133-6143.
Smyshlyaev, V.P., Fleck, N.A., 1996. The role of strain gradients in the grain size effect for polycrystals. Journal of the Mechanics and Physics of Solids 44 (4), 465-495.

Stölken, J.S., Evans, A. G., 1998. A microbend test method for measuring the plasticity length scale. Acta Materialia 46 (14), 5109-5115.

J. G. Swadener, E. P. George, G. M. Pharr, 2002. The correlation of the indentation size effect measured with indenters of various shapes. Journal of the Mechanics and Physics of Solids 50 (4), 681-694.

Van Rompaey, T., Lani, F., Jacques, P.J., Blanpain, B., Wollants, P., Pardoen, T., 2006. Three-dimensional computational-cell modeling of the micromechanics of the martensitic transformation in transformation-induced-plasticity-assisted multiphase steels. Metallurgical and Materials Transactions A 37 (1), 99-107.

List of Tables

List of Figures

Table 1: Material parameters

	Ferrite	Austenite	Martensite
E(GPa)	200	187	200
σ_{y_0}(MPa)	475	700	2000
ϵ_0	55	50	800
N	0.27	0.3	0.05

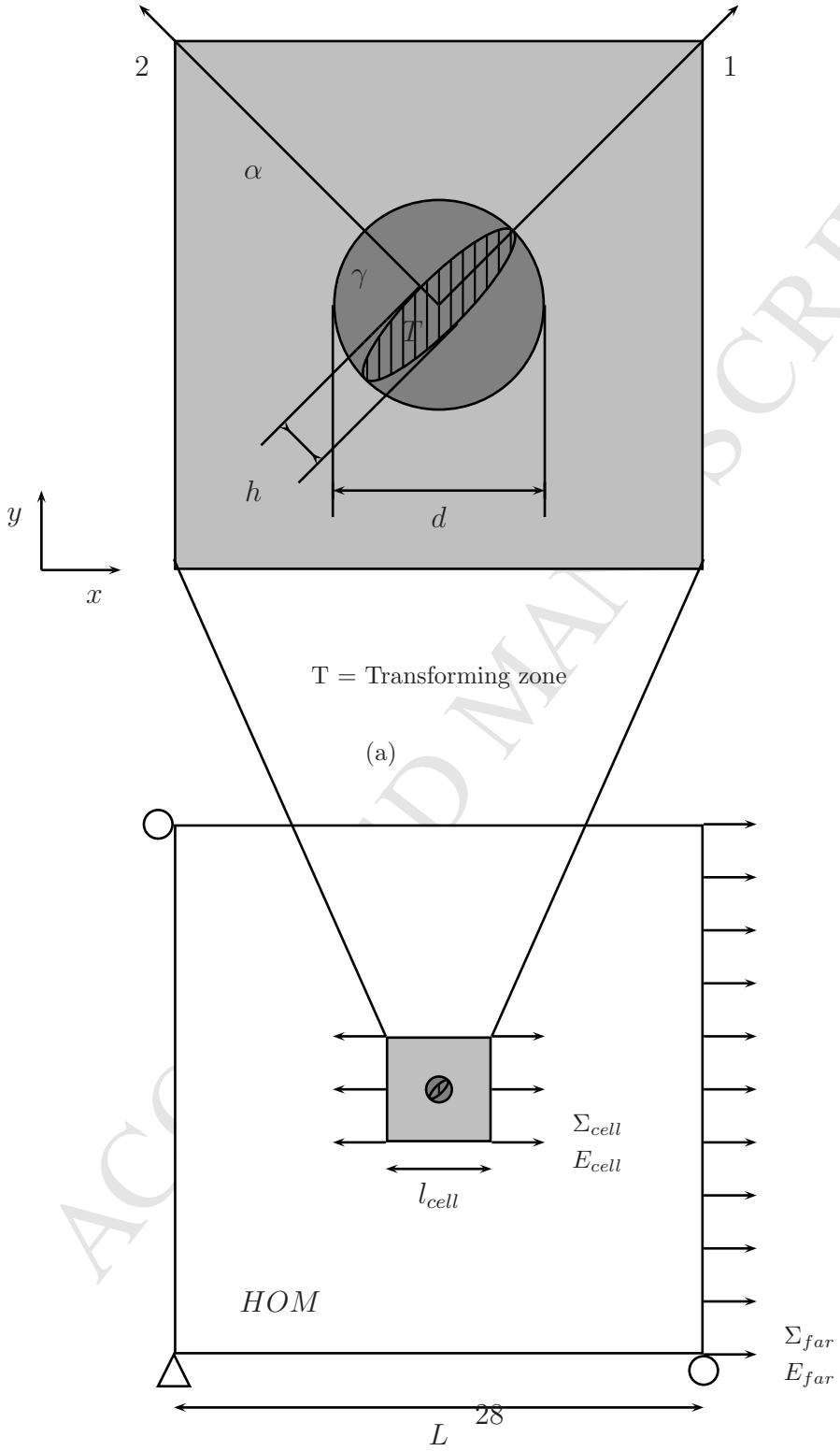

Figure 1: Schematic drawing of the simplified microstructure representative volume element: (a) geometrical parameters (b) embedded cell model.

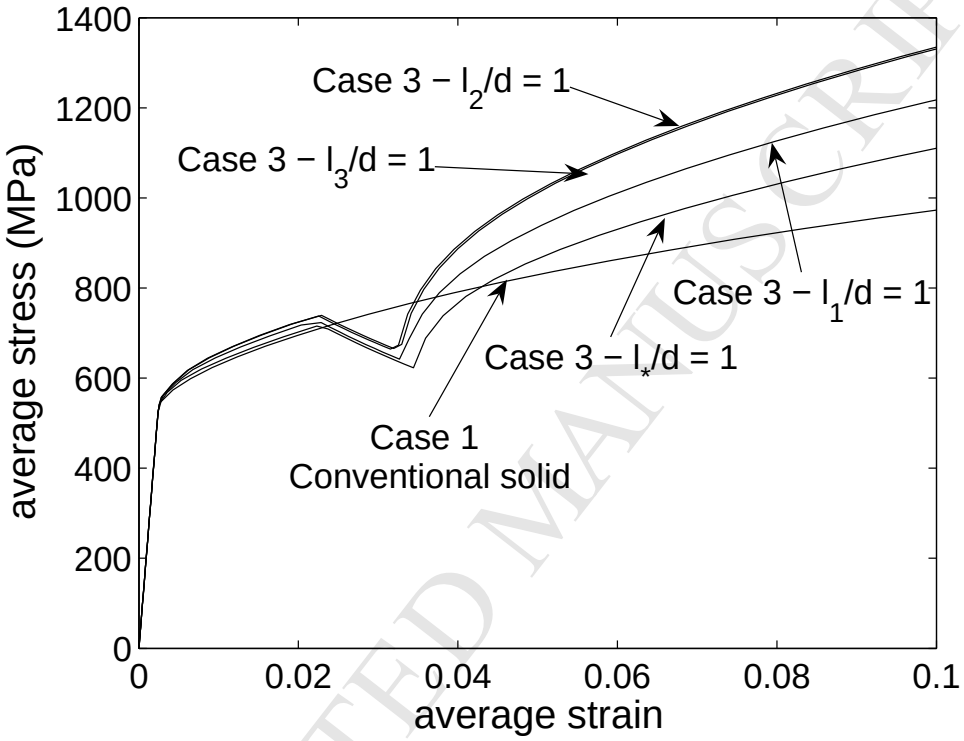

Figure 2: Overall stress strain response along the tensile direction of the embedded unit cell with constrained plastic flow at the $\alpha^{'}/\gamma$ interface and unconstrained plastic flow at elasto-plastic boundaries, $\gamma^{tsf} = 20\%$, in cases n°1, and n°3 with the single parameter model, characterized by the ratio $l_*/d = 1$ and the multi-parameter model characterized by l_1/d, l_2/d and l_3/d all equal to 0 except for one equal to 1.

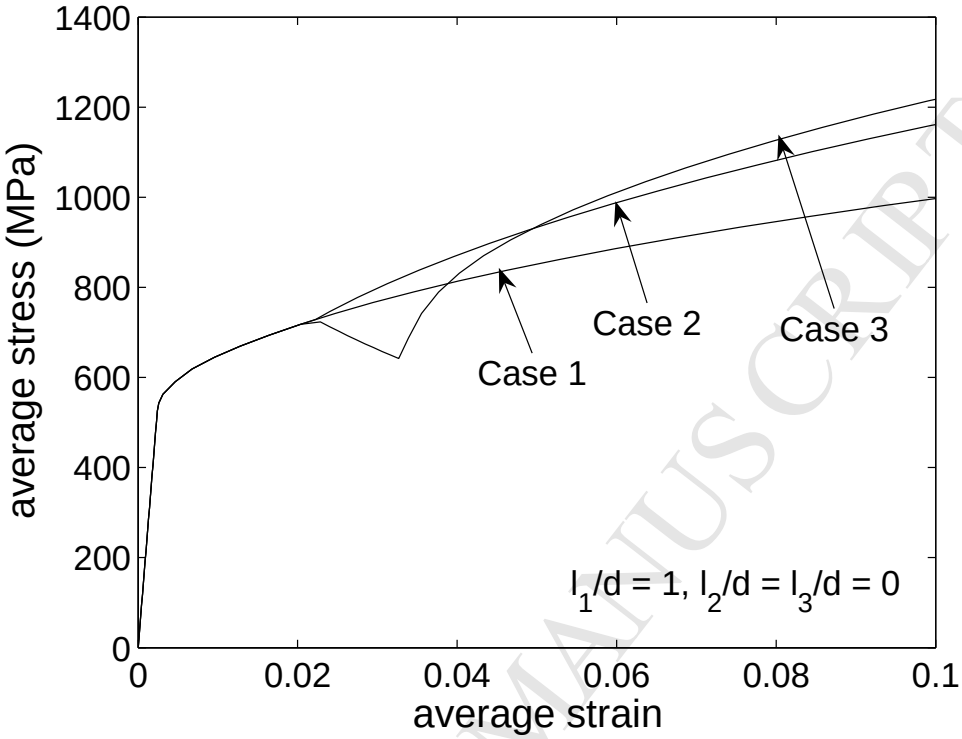

(a)

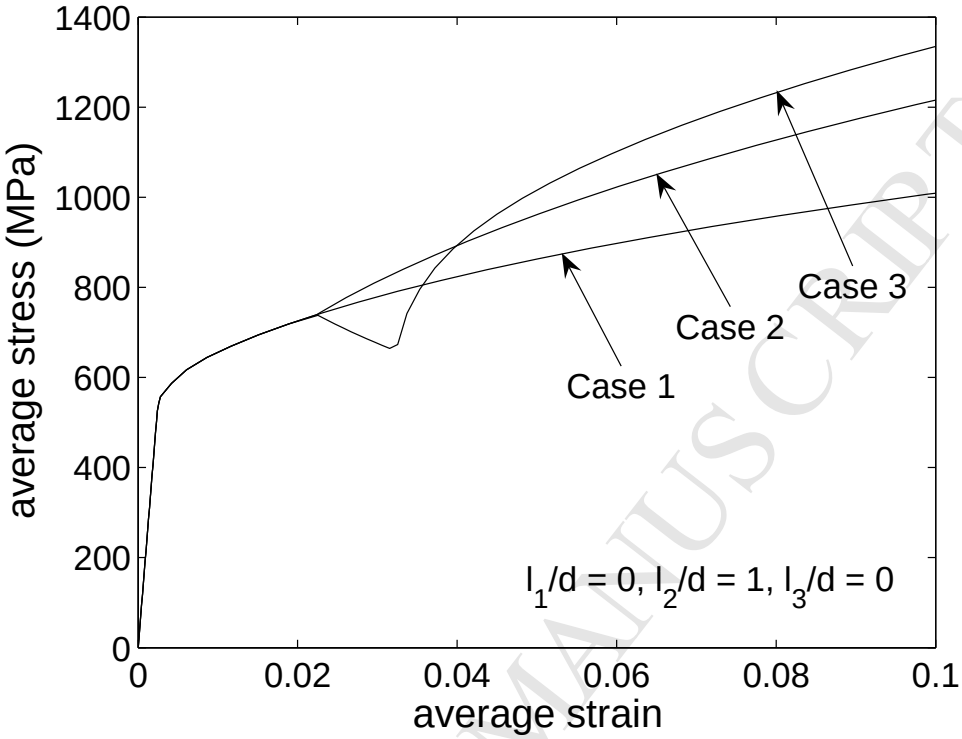

(b)

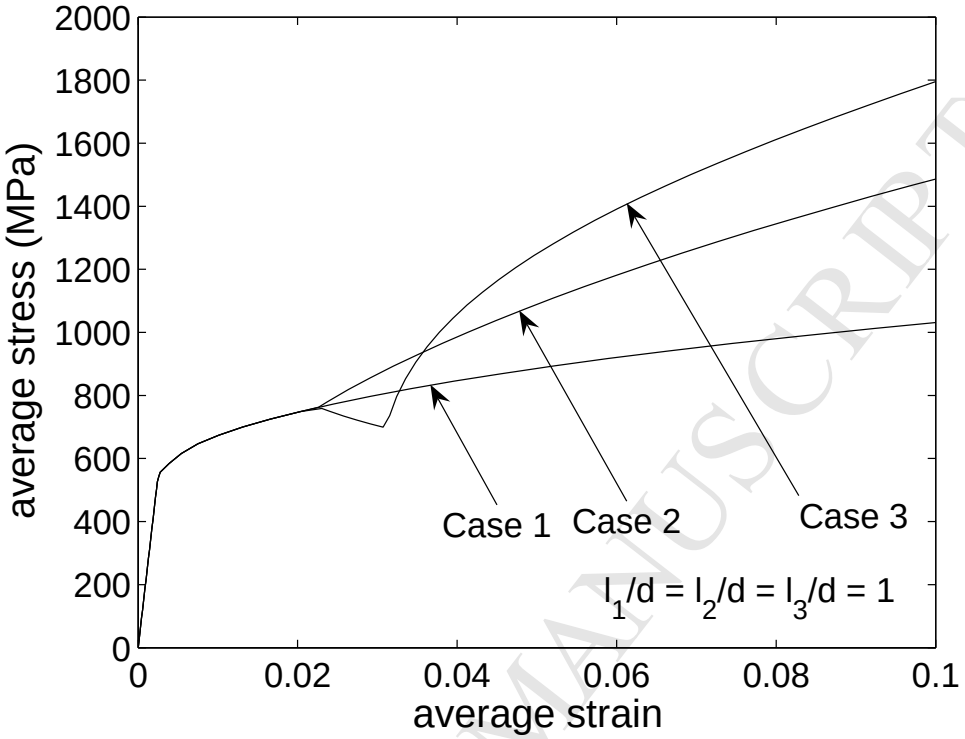

(c)

Figure 3: Stress strain response along the tensile direction of the embedded unit cell with constrained plastic flow at the $\alpha^{'}/\gamma$ interface and unconstrained plastic flow at elasto-plastic boundaries, $\gamma^{tsf} = 20\%$, in cases n°1, n°2, n°3 with the multi-parameter model characterized by (a) $l_1/d = 1$ and $l_2/d = l_3/d = 0$; (b) $l_1/d = 0, l_2/d = 1$ and $l_3/d = 0$ and (c) $l_1/d = l_2/d = l_3/d = 1$.

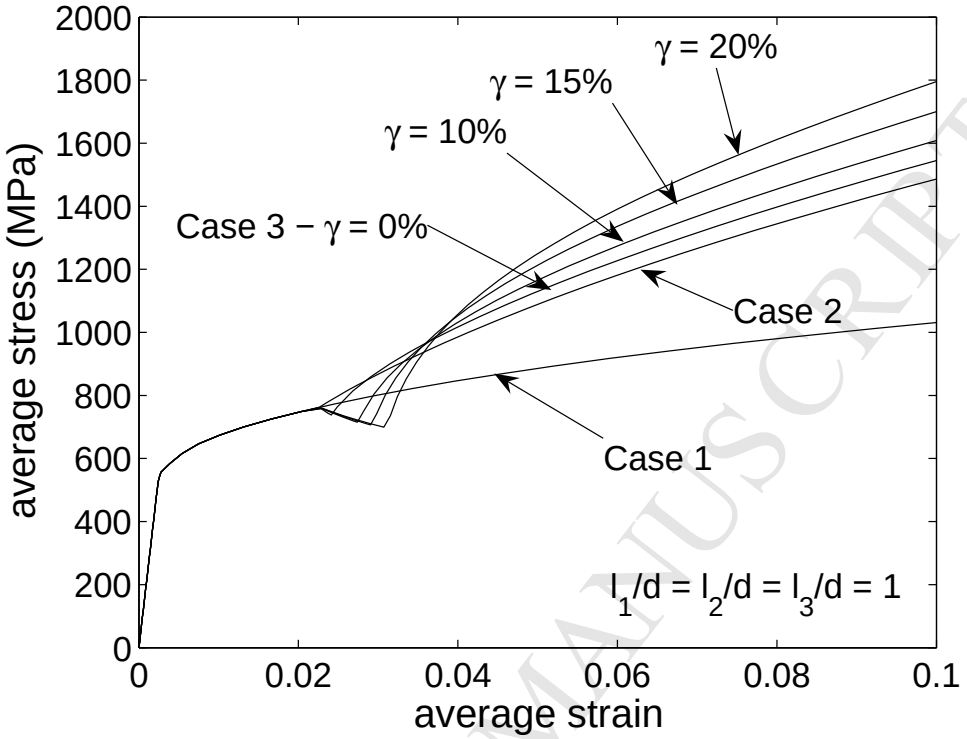

Figure 4: Effect of the shear component of the transformation strain γ_{tsf} on the stress strain response along the tensile direction of the embedded unit cell with constrained plastic flow at the $\alpha^{'}/\gamma$ interface and unconstrained plastic flow at elasto-plastic boundaries, $l_1/d = l_2/d = l_3/d = 1$, for cases n°1, n°2, n°3.

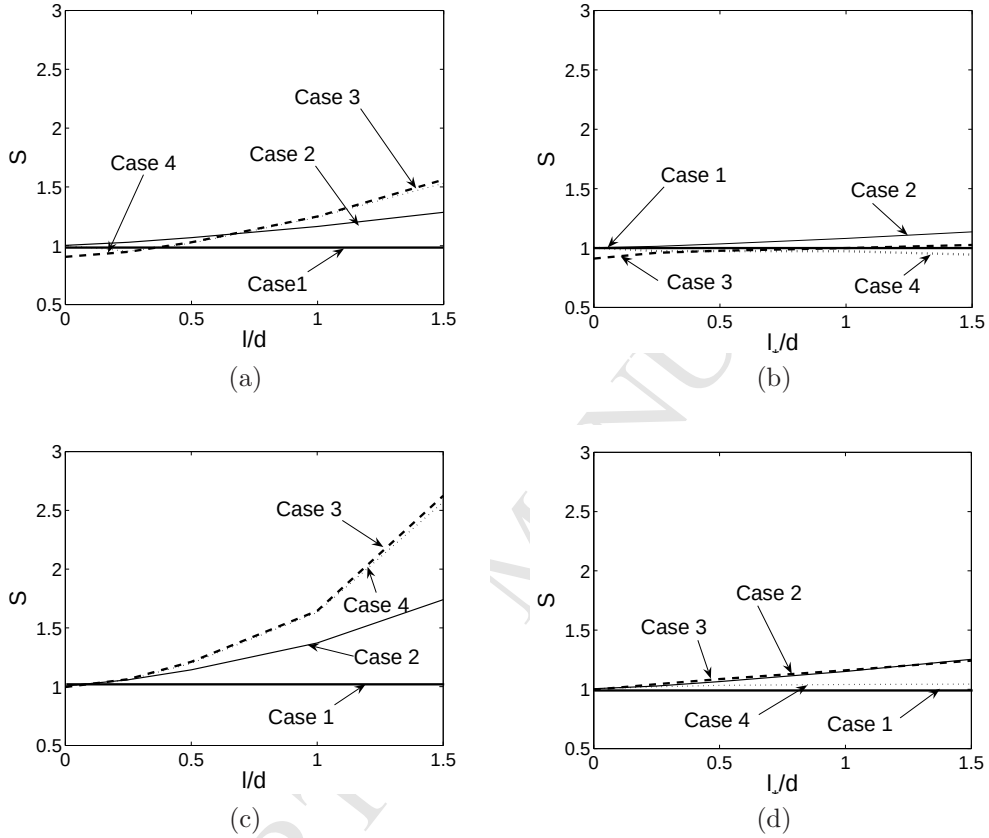

Figure 5: Variation of the strengthening indicator S with constrained plastic flow at the $\alpha^{'}/\gamma$ interface and unconstrained plastic flow at elasto-plastic boundaries, $\gamma^{tsf} = 20\%$ as a function of (a) $l/d = l_1/d = l_2/d = l_3/d$ at $E_{macro} = 4\%$; (b) l_*/d (single parameter theory) at $E_{macro} = 4\%$; (c) $l/d = l_1/d = l_2/d = l_3/d$ at $E_{macro} = 8\%$; and (d) l_*/d at $E_{macro} = 8\%$; for cases n°1, n°2, n°3 and n°4.

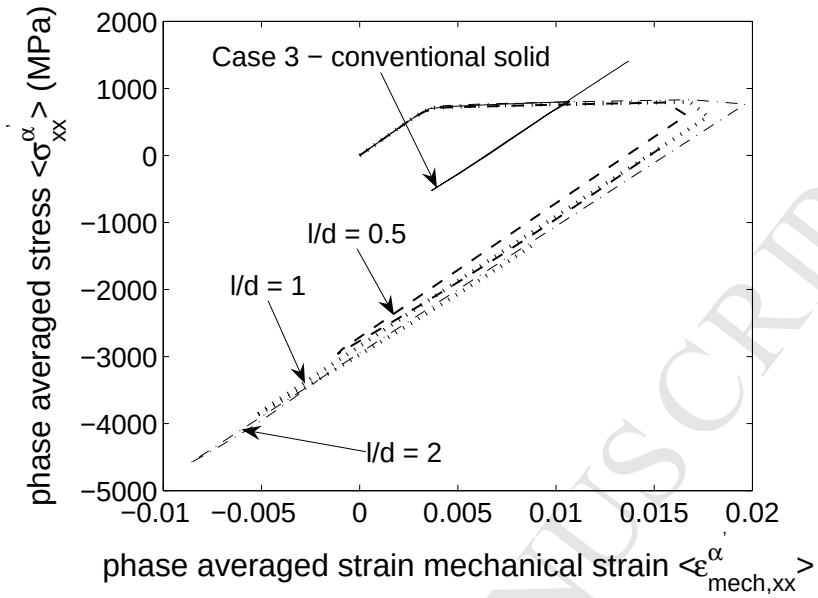

(a)

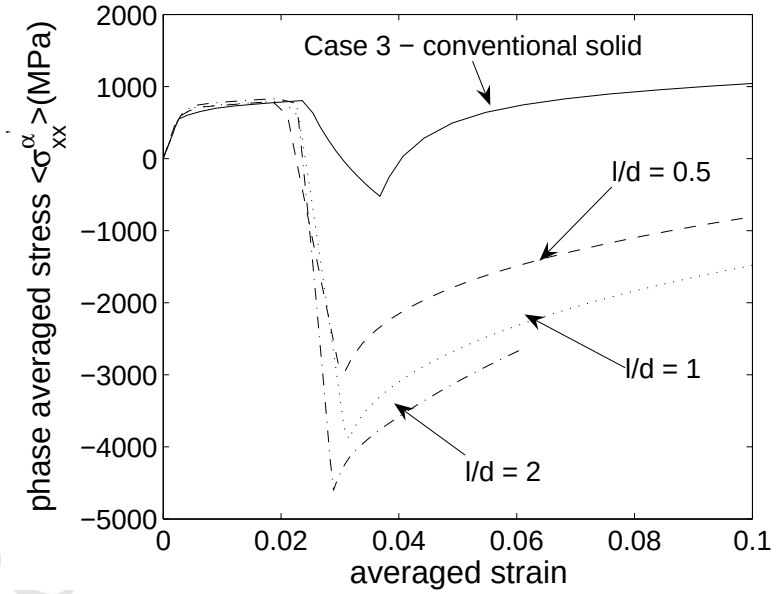

(b)

Figure 6: Variation of the phase averaged stress in the martensite as function of (a) the phase averaged strain and of (b) the averaged strain E for various ratios $l/d = l_1/d = l_2/d = l_3/d$ using $\gamma^{tsf} = 20\%$ for case n°3 only.

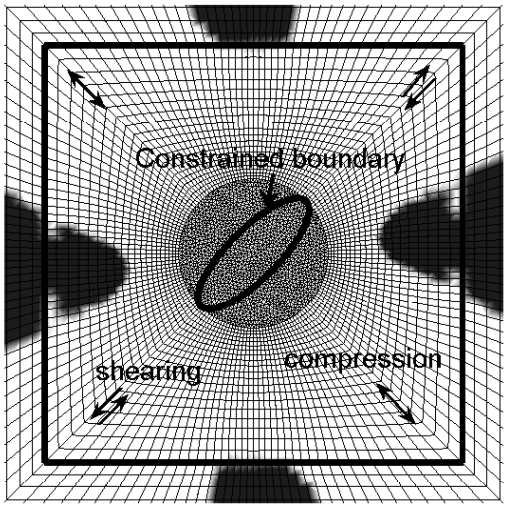

Figure 7: Repartition, at the end of the transformation step, of the elastic unloading zones, using $l_1/d = l_2/d = l_3/d = 1$, $\gamma^{tsf} = 20\%$ in case n°3. The plastic flow is always fully constrained at the $\alpha^{'}/\gamma$ interface. The limit between the unit cell and the homogenized medium is indicated by the black box.

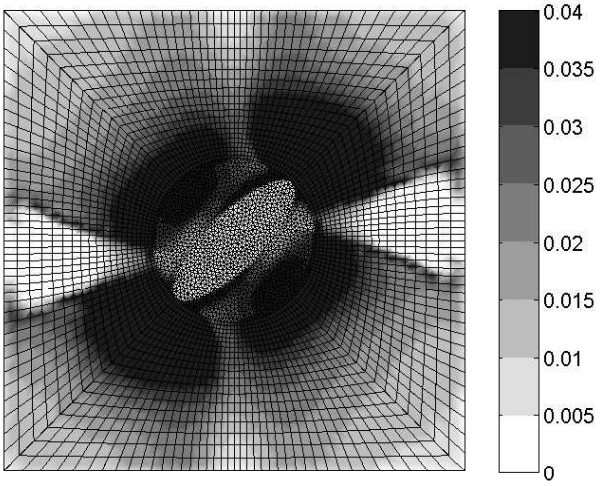

Figure 8: Repartition, at the end of the transformation step, of the variation since the start of the transformation of the generalized effective plastic strain, using $l_1/d = l_2/d = l_3/d = 1$, $\gamma^{tsf} = 20\%$ in case n°3. The plastic flow is always fully constrained at the $\alpha^{'}/\gamma$ interface.